Q-Band ENDOR (Electron Nuclear Double Resonance) of the High-Affinity Ubisemiquinone Center in Cytochrome bo_3 from *Escherichia coli*†

Andrei V. Veselov,‡ Jeffrey P. Osborne,§ Robert B. Gennis,§ and Charles P. Scholes*,‡

Department of Chemistry, University at Albany, SUNY, Albany, New York 12222, and Department of Chemistry, Chemical & Life Sciences Laboratory, 600 South Mathews Avenue, University of Illinois, Urbana, Illinois 61801

Received November 22, 1999

ABSTRACT: Electron nuclear double resonance (ENDOR) was performed on the protein-bound, stabilized, high-affinity ubisemiquinone radical, $Q_H^{\bullet-}$, of bo_3 quinol oxidase to determine its electronic spin distribution and to probe its interaction with its surroundings. Until this present work, such ENDOR studies of protein-stabilized ubisemiquinone centers have only been done on photosynthetic reaction centers whose function is to reduce a ubiquinol pool. In contrast, $Q_H^{\bullet-}$ serves to oxidize a ubiquinol pool in the course of electron transfer from the ubiquinol pool to the oxygen-consuming center of terminal bo_3 oxidase. As documented by large hyperfine couplings (>10 MHz) to nonexchangeable protons on the $Q_H^{\bullet-}$ ubisemiquinone ring, we provide evidence for an electronic distribution on $Q_H^{\bullet-}$ that is different from that of the semiquinones of reaction centers. Since the ubisemiquinone itself is physically nearly identical in both $Q_H^{\bullet-}$ and the bacterial photosynthetic reaction centers, this electronic difference is evidently a function of the local protein environment. Interaction of $Q_H^{\bullet-}$ with this local protein environment was explicitly shown by exchangeable deuteron ENDOR that implied hydrogen bonding to the quinone and by weak proton hyperfine couplings to the local protein matrix.

Ubiquinone binding sites which act as transformers between one-electron and two-electron redox processes are found in respiratory and photosynthetic complexes. Such sites often stabilize a singly reduced, paramagnetic semiquinone anion ($Q^{\bullet-}$,[1] where asterisked protons are those probed by ENDOR).

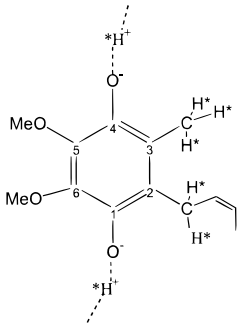

Selective binding of the semiquinone to a protein site allows the reactive semiquinone species to be spatially confined and to be controlled by its surroundings so that the semiquinone can function more effectively in electron-transfer and proton-transfer kinetics. When paramagnetic semiquinone is stabilized, the thermodynamic implication is that the two one-electron couples, quinone/semiquinone ($Q/Q^{\bullet-}$) and semiquinone/hydroquinol ($Q^{\bullet-}/QH_2$), are equalized (*1*). The prediction of sites to stabilize ubisemiquinone is a feature of Q cycles (*2*, *3*).

The best delineated, tightly bound quinone sites to date have been the ubiquinone-10 Q_A and Q_B electron acceptor sites of the purple bacterial photosynthetic reaction center. These sites function to reduce the ubiquinol pool. At the tightly bound ubiquinone of Q_A, reducing equivalents are received in one-at-a-time fashion from photooxidized chlorophyll and transferred to ubiquinone of Q_B for ultimate release of these equivalents into the reduced ubiquinol pool. Q_A and Q_B also function to couple transmembrane electronic charge separation to the production of a transmembrane proton gradient to be used for bioenergetics (*4*). The protein structure at both Q_A and Q_B, including the position of nearby nitrogenous hydrogen bonding partners and the position of an intervening Fe^{2+}, is known from X-ray crystallographic work on the reaction centers from *Rps. viridis* (*5*) and *Rb. sphaeroides* (*6*, *7*). A light-induced change in the Q_B ubiquinone conformation has been noted (*8*). Primarily because of detailed EPR−ENDOR studies, the electronic spin distribution from the highly stabilized $Q_A^{\bullet-}$ and $Q_B^{\bullet-}$ ubisemiquinone anions, studied after the paramagnetic intervening Fe^{2+} had been replaced by diamagnetic Zn^{2+}, is also the best resolved of any biological semiquinone center to date (*9*−*11*). The ENDOR studies on $Q_A^{\bullet-}$ and $Q_B^{\bullet-}$ were combined with deuteration of solvent, protein, or quinone and with variation in the quinone ring substituents. These

† Supported by the National Institutes of Health (Grant GM-35103 to C.P.S.) and by a grant from the U.S. Department of Energy (DEFGO2-87ER13716 to R.B.G.).

* To whom correspondence should be addressed. Telephone: (518) 442-4551; Fax: (518) 442-3462; E-mail: cps14@cnsvax.albany.edu.

‡ University at Albany.

§ University of Illinois.

[1] Abbreviations: ptp, peak-to-peak; G, gauss; kG, kilogauss; I.D., inside diameter; O.D., outside diameter; EPR, electron paramagnetic resonance; ENDOR, electron nuclear double resonance; ESEEM, electron spin−echo envelope modulation; μW, microwatt; nW, nanowatt; RF, radio frequency. Q_A and Q_B are the ubiquinone binding centers of the photosynthetic reaction center; $Q_A^{\bullet-}$ and $Q_B^{\bullet-}$ are the ubisemiquinone radical anions in these centers. Q_H is the high-affinity ubiquinone binding center of bo_3 quinol oxidase; $Q_H^{\bullet-}$ is the ubisemiquinone radical anion in this center.

10.1021/bi9926835 CCC: $19.00
Published on Web 02/24/2000

studies provided hyperfine information on electron spin densities at the C(3) methyl and C(2) β-methylene isoprenyl protons, on hydrogen-bonded protons connecting the ubiquinone oxygen(s) to the protein, and on surrounding protons of the protein matrix (*9, 10*). There was evidence from nitrogen ESEEM that showed proximity and hyperfine coupling of nearby ^{14}N nitrogens and indicated hydrogen bonding between the quinone oxygens and nearby histidine and amide nitrogens (*12*). The work on $Q_A^{\bullet-}$ and $Q_B^{\bullet-}$ of the bacterial reaction centers has led to ENDOR and ESEEM study of analogous plastoquinone sites of photosystem II (*13*−*16*) and of a phylloquinone site of photosystem I (*17*−*19*). This recent work has focused on finding proton and nitrogen spectroscopic evidence for hydrogen bonding that stabilizes the semiquinone form and may cause its spin densities to change from those found for semiquinone anion in solvent.

Quinone binding sites have been categorized as reduction (acceptor) sites, oxidation (donor) sites, and electron-pair splitting sites (*1*). The Q_A−Q_B sites of photosynthetic reaction centers are reductive (acceptor) sites. There are other reduction sites whose structure is not yet delineated, such as the Q_s site of succinate dehydrogenase (*20*) and the Q_n site of NADH dehydrogenase (*21*). In the cytochrome bc_1 complex, ubiquinol is oxidized at the Q_o site, near the positive side of the inner mitochondrial membrane, and quinone is reduced at the Q_i site, near the negative side of the membrane (*22, 23*). This electron flow is coupled by ubiquinol to translocation of protons across the mitochondrial membrane. The combination of Q_o and Q_i sites in the bc_1 complex leads to a bifurcation (*24*) or splitting in the flow of a pair of electrons from the incoming ubiquinol. By use of inhibitors which selectively bind in place of ubiquinone, the physical location of the Q_o and Q_i sites has been inferred but is yet to be pinpointed from crystal structures of the bc_1 complex (*25, 26*).

For aerobic respiration, *E. coli* uses electrons from ubiquinol (Q-8), rather than from ferrocytochrome *c*, to reduce dioxygen at a heme−copper (o_3−Cu_B) binuclear center (*27*−*29*). To accomplish the redox coupling of oxygen reduction to the source of reducing equivalents in the ubiquinol pool, a strongly bound ubisemiquinone site, Q_H, acts as an "oxidative transformer" between the two-electron oxidation of the ubiquinol pool and the one-electron (at-a-time) reduction of oxygen at the heme−copper center (*30*). This Q_H site that we study stabilizes ubisemiquinone $Q_H^{\bullet-}$ and ubiquinol, whereas Q_A stabilizes ubiquinone and ubisemiquinone (*31*). The strongly bound, high-affinity ubiquinone is retained during enzyme preparation (*32*), and the semiquinone form is highly stabilized at this site (*1, 31*). There is also a low-affinity quinone binding site whose quinone may exchange with the ubiquinol pool (*30*). A straightforward explanation of the bioenergetic role of Q_H is that all electrons transferred through it from the ubiquinol pool are used to reduce oxygen at the heme−copper binuclear center where the free energy of this reduction is coupled to proton pumping (*30, 32*). However, it has been suggested that Q_H may function as part of a pair splitter in a Q-cycle (after the fashion of Q_o and Q_i in the bc_1 complex), where, for each ubiquinol oxidized, one electron is cycled back to the ubiquinol pool while the other electron is sent to the heme−copper binuclear center (*33, 34*).

A strong ubisemiquinone EPR signal has been observed from bo_3 at X-band, and unlike signals of the protein-bound $Q_A^{\bullet-}$ and $Q_B^{\bullet-}$ ubisemiquinone anions of the bacterial photosynthetic reaction centers, this signal has shown partially resolved hyperfine structure with splittings of approximately 4 G (*1, 31*). As shown here, $Q_H^{\bullet-}$ has *g* values, as measured with Q-band EPR, typical of ubisemiquinone anion. Until now $Q_A^{\bullet-}$ and $Q_B^{\bullet-}$ in the bacterial photosynthetic apparatus are the only protein-bound ubisemiquinone anions whose electronic structure has been determined with the high resolution of ENDOR−EPR and whose physical structure within a protein environment is known from X-ray crystallography. The function of the Q_H ubisemiquinone of bo_3 oxidase is markedly different from that of the ubiquinones of photosynthetic reaction centers. In light of the functional difference, the purpose of our present study is to contrast hyperfine couplings and underlying electronic structure inferred from the ENDOR signal of the $Q_H^{\bullet-}$ anion of bo_3 oxidase with the corresponding information on photosynthetic semiquinone anions, for which assignments of ring methyl, ring β-methylene isoprenyl, and exchangeable protons have been made and for which the local protein structure is better known.

EXPERIMENTAL PROCEDURES

Materials. Cytochrome bo_3 was made by the method of ref *35* with modifications detailed in ref *36*. The detergent conditions served to remove weakly bound ubiquinone but to leave the strongly bound ubiquinone at the high-affinity Q_H center. The concentration of enzyme for these studies was approximately 0.8 mM. In preparation for anaerobic reduction, samples were repeatedly pump-flushed with pure argon. By stoichiometric addition of NADH (Sigma) in the presence of 3 μM PMS (phenazine methosulfate), the enzyme was anaerobically reduced at pH 7.4 in 100 mM HEPES buffer containing 0.1% *n*-dodecyl-β-D-maltoside detergent (Anatrace, Inc., Maumee, OH) with approximately 2 e^- per molecule. The sample of ~50 μL volume was transferred by an argon-flushed, gastight Hamilton syringe to an argon-flushed Q-band sample tube (2.0 mm I.D., 2.4 mm O.D.; VitroCom Inc., Mountain Lakes, NJ), and frozen under the argon atmosphere by plunging into liquid nitrogen. Deuteration to approximately 90% was carried out vs pD 7.6 100 mM HEPES buffer by ultrafiltration with a Microcon 3 concentrator (Millipore, Burlington, MA) over a period of several hours at 4 °C. For ongoing studies which included both this ubisemiquinone-focused study and a separate study underway on the heme o−Cu_B center, the total stock available was 0.8 mL. Thus, it was critical to use small (~50 μL) Q-band samples, and the potential for pH and electrochemical manipulation was limited.

Methods. Q-band (34 GHz) ENDOR measurements were performed at both 90 and 2.1 K with a cryogenically tunable TE_{011} Q-band resonator (*37*) located in an immersion double dewar (Janis, Inc., Wilmington, MA) which was filled with pumped liquid helium at 2.1 K and with He exchange gas at 90 K. ENDOR was obtained under rapid-passage (χ') conditions with 100 kHz field modulation (*38*) in the 1−2 G (ptp) range for resolving couplings >2 MHz and 0.15 G (ptp) for resolving couplings <2 MHz. The ENDOR RF field typically had a ptp amplitude of 1 G. The microwave power at 90 K was 27 μW, and at 2.1 K it was in the 2−100 nW

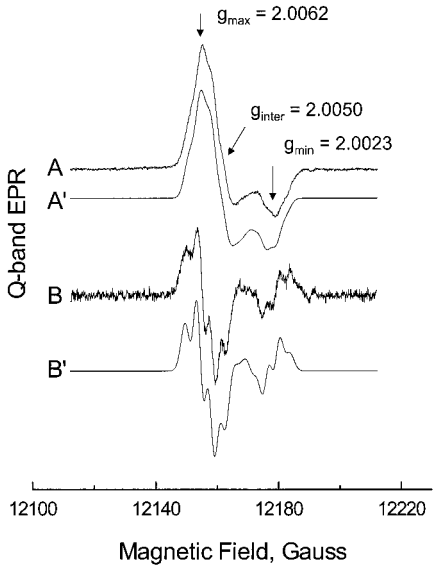

FIGURE 1: Spectrum A provides the first-derivative ($d\chi''/dH$) Q-band EPR spectrum at $T = 90$ K, $\nu_e = 34.1304$ GHz, with 100 kHz field modulation of 1.2 G ptp, and 8.3 μW microwave power. This sample was prepared in protonated solvent. Spectrum B shows the second-derivatve ($d^2\chi''/dH^2$) EPR spectrum obtained by taking a numerical derivative of spectrum A. Simulations A′ (first derivative) and B′ (second derivative) using Bruker's WINEPR SimFonia software package were carried out with the following set of parameters: g_x, g_y, $g_z = 2.0060$, 2.0054, 2.0025; A_{xx}, A_{yy}, $A_{zz} = 10$, 12, 9 MHz with 3 equivalent protons having this hyperfine tensor; Gaussian packet widths between derivative extrema having W_x, W_y, $W_z = 3.1$, 4.2, 3.1 G.

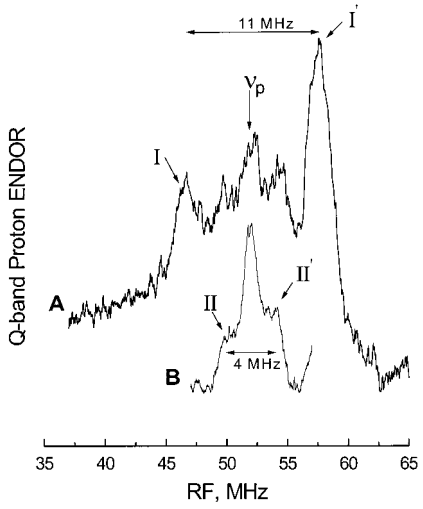

FIGURE 2: This figure shows the Q-band ENDOR signal at 90 K under dispersion rapid passage conditions. Features labeled I, I′ had splittings of about 11 MHz, and features labeled II, II′ had splittings of about 4 MHz. Spectrum A was taken with a system time constant = 0.16 s, RF sweep rate = 3 MHz/s, microwave power = 26 μW, 100 kHz modulation = 2.4 G ptp, magnetic field = 12.162 kG, $\nu_e = 34.137$ GHz, $g = 2.0055$, and overall signal averaging time of 3/4 h. The RF power was pulsed with a 10% duty cycle (10 μs on and 90 μs off). Spectrum B was taken under the same conditions as spectrum A, except for a smaller 100 kHz field modulation of 1.2 G ptp; this latter spectrum took 3 h of signal averaging.

range. For proton ENDOR spectra, one expects two lines for each magnetic nucleus to appear symmetrically spaced, to first order, about the nuclear Larmor frequency, ν_P, and separated by the respective proton hyperfine coupling, A. The ENDOR frequencies, ν_{ENDOR}, are given by $\nu^{\pm}_{ENDOR} = |\nu_P \pm A/2|$. EPR frequencies were measured with an EIP model 548 microwave frequency counter (San Jose, CA); g values were calibrated versus a DPPH (2,2-diphenyl-1-picrylhydrazyl, Sigma) sample having a known g value of 2.0036. Powder pattern EPR spectral simulations were carried out with WINEPR SimFonia Version 1.25 software from Bruker Analytische Messtechnik GmbH.

RESULTS

EPR. Q-band EPR obtained at 90 K (Figure 1) gave g values characteristic of the ubisemiquinone anion radical (*39*). By a double integration comparison with a sample of TEMPO (2,2,6,6-tetramethyl-4-piperidinol, Sigma) of known concentration, the concentration of the ubisemiquinone anion radical was determined to be ~250 μM. The g values shown in Figure 1A are g values experimentally measured respectively at the low-field derivative extremum, the intermediate-field derivative zero crossing, and the high-field extremum to give empirical estimates of $g_x = 2.0062 \pm 0.0001$, $g_y = 2.0050 \pm 0.0001$, and $g_z = 2.0023 \pm 0.0001$. The g values of the same features in the reaction center ubisemiquinone spectrum of ref *39* were $g_x = 2.0064$, $g_y = 2.0050$, and $g_z = 2.0023$. Explicit resolution of more precise g_x and g_y values will require higher frequency EPR such as W-band (92 GHz) EPR (*40*). We noted inflections clarified by a second-derivative presentation (Figure 1B) that indicated hyperfine couplings. Such inflections occurred in samples made in both protonated and deuterated solvent. The splitting between second-derivative features was about 4 G. Detailed simulations shown in Figure 1A′,B′ (also see Discussion) required three equivalent protons with a coupling of about 4 G (~11 MHz), consistent with ENDOR results, to reproduce the splittings.

ENDOR. Most of the ENDOR work reported on $Q_A^{\bullet-}$ and $Q_B^{\bullet-}$ of photosynthetic reaction centers has been done at liquid nitrogen temperatures and above (*9*, *10*, *41*), temperatures at which rapid methyl rotation and motional averaging of the methyl proton features persist. Because the electron spin relaxation times for cupric and ferric transition metals are too short for ENDOR study at 90 K, the potential for unwanted, overlapping ENDOR signals of heme o_3 or Cu_B was eliminated at 90 K. With our Q-band ENDOR system, we found that the rapid passage method carried out in the dispersion mode with 100 kHz field modulation, as opposed to the more commonly used frequency modulated absorption method, gave us superior signal-to-noise for protons with broad (~1 MHz wide) signals and large hyperfine couplings. Figure 2A, taken at g_y over a 30 MHz range centered at the free proton frequency, brought out nonexchangeable features I, I′ with ~11 MHz splitting and II, II′ with ~4 MHz splitting. A coupling of 11 MHz translates into a hyperfine splitting of ~4 G, like that observed at X-band (ref *1*, Figure 1a,c) and like that resolved with our second-derivative presentation of Q-band EPR. The features II, II′ with smaller couplings of approximately 4 MHz are accented in Figure 2B, where they were obtained under smaller field modulation with more signal averaging and higher resolution than Figure 2A.

In bacterial photosynthetic reaction centers prepared for EPR and ENDOR with diamagnetic Zn^{2+} rather than

paramagnetic Fe^{2+} (*39*, *42*), the radical signals of $Q_A^{\bullet-}$ and $Q_B^{\bullet-}$, having no nearby paramagnetic relaxer, saturate very readily; the result can be a very broad and distorted ENDOR signal at liquid helium temperature (R. A. Isaacson, personal communication). The ubisemiquinone signal of bo_3 certainly was easier to saturate than a transition metal signal, but the ubisemiquinone ENDOR signal at 2.1 K was not exceptionally broadened or distorted from its appearance at 90 K, possibly because there are other potential spin-relaxing metal centers in bo_3 oxidase. Although tunneling behavior of methyl group protons may provide motion even at liquid helium temperature (*43*), spectral broadening may result from freezing out of methyl rotations. The lower helium temperature might slow the rotation of the methyl group, but it provided much better signal-to-noise compared to 90 K for doing ENDOR.[2] At 2.1 K, the ENDOR signals which we report here were signals that only occurred over the limited range of the $QH^{\bullet-}$ signal and except for better signal-to-noise were similar in appearance to the $QH^{\bullet-}$ signals observed at 90 K. Thus, we measured ENDOR from $QH^{\bullet-}$ at pumped liquid helium temperatures with excellent signal-to-noise and good resolution so that changes in the couplings of features I, I′ and II, II′ over the entire g_x-g_z range could be followed. (Adequate signal-to-noise at 90 K was at best only obtained at the intermediate g value, g_y, where the EPR and ENDOR signals are largest.) Figure 3 shows that the features I, I′ had couplings which varied from a maximum of about 13 MHz in the g_x-g_y region to ~9.5 MHz at g_z, while the features II, II′ had couplings which diminished from 4−5 MHz at g_x-g_y to <3 MHz at g_z. An expanded, detailed variation of feature I′ versus g value is provided in Figures S1 and S2 of the Supporting Information. Figure 4 shows the variation in proton couplings closer to the free proton frequency as a function of g value; the outlying features II, II′ with coupling 4−5 MHz at the largest g values diminished in their spread and their couplings to ~3 MHz as the overall pattern shifted inward at the lowest g value (2.0023). Comparison of the protonated and deuterated samples indicated weakly resolved evidence for exchangeable protons in the 4−5 MHz region as well. At low g values, there was an additional exchangeable feature (starred in Figure 4) which had a coupling of ~1.8 MHz.

To show more definitively that $QH^{\bullet-}$ had exchangeable proton/deuterium features, we performed deuterium ENDOR. Deuterium ENDOR from our samples can only come from exchangeable deuterium, and it will have no overlap with nonexchangeable features. The resultant deuterium ENDOR splitting, as shown in Figure 5, was 0.8 MHz. The 0.8 MHz coupling to a deuterium would correspond to an exchangeable proton coupling of 5.2 MHz.

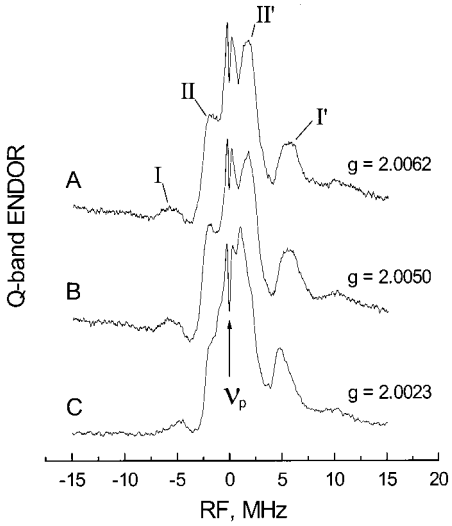

FIGURE 3: This figure presents the Q-band ENDOR signal of protons taken at $T = 2.1$ K over a 30 MHz range centered at the free proton frequency, ν_P, to show anisotropy of nonexchangeable proton hyperfine couplings, especially those labeled I, I′. The g values where spectra were measured were $g_x = 2.0062$ (A), $g_y = 2.0050$ (B), and $g_z = 2.0023$ (C). Experimental conditions were 100 kHz modulation = 1.2 G ptp, system time constant = 0.02 s, RF sweep rate = 3 MHz/s over a 30 MHz range, microwave power = 2.5 nW. The RF power was pulsed with a 10% duty cycle (10 μs on and 90 μs off). These spectra took 10−20 min of signal averaging each. See Figures S-1 and S-2 for an expanded view of the frequency variation of feature I′ versus g value.

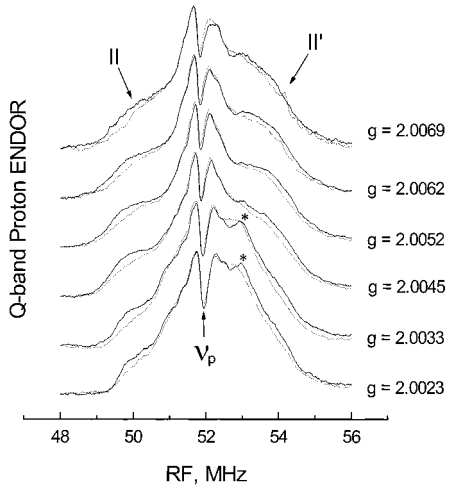

FIGURE 4: This figure presents the Q-band ENDOR signal of protons taken over an 8 MHz range centered at the free proton frequency especially to show the decrease in the splitting of features II, II′ as the g-value diminished. Experimental conditions were $T = 2.1$ K, 100 kHz modulation = 0.3 G ptp, system time constant = 0.04 s, RF sweep rate = 2 MHz/s over an 8 MHz range, microwave power = 2.5 nW, $\nu_e = 34.12$ GHz. The solid line spectra are from the protonated sample, and the dotted spectra are from the deuterated sample.

Finally, the details of the weak couplings a,a′; b,b′; and c,c′ with respective magnitudes of 0.09, 0.27, and 0.50 MHz were also better resolved as shown in Figure 6; a derivative presentation corresponding to Figure 6 is presented in Figure S-3 of the Supporting Information. Detailed study with various combinations of deuterated protein and deuterated quinones (*10*) established that such weak couplings were due

[2] A broad, weak feature approximately 10.2 MHz above the free proton frequency was noted at 2.1 K. It was not observed at 90 K. It could be a distortion due to rapid passage. If real, this feature would belong to a proton having a coupling of ~20.5 MHz or 7.3 G. Such a 7.3 G coupling is inconsistent with the experimental Q-band EPR liquid nitrogen temperature line shape of the ubisemiquinone whose features were sufficiently detailed that a 7.3 G hyperfine coupling would have been highly evident; no such 7.3 G coupling was required in the simulation of its liquid nitrogen temperature line shape. It is possible that a methyl group conformation could be locked in at liquid helium temperatures, and that this conformation has a larger hyperfine coupling than ~11 MHz for one of its protons. If the C2−C3−Cβ−Hβ methyl dihedral angles of $\theta = 45°$, 165 °, and −75° happened to be frozen in at 2.1 K, then the methyl proton couplings would be in the ratio of 11:20.2:1.6 MHz at 2.1 K, where the 1.6 MHz feature could be obscured by numerous other weakly coupled protons.

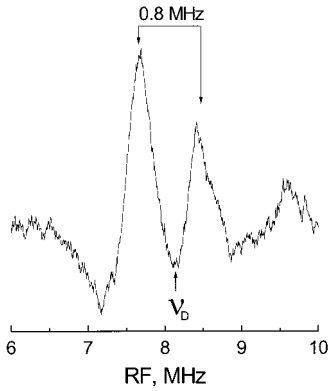

FIGURE 5: This figure is the Q-band ENDOR signal of exchangeable deuterium. Experimental conditions were $T = 2.1$ K, 100 kHz modulation = 0.6 G ptp, system time constant = 0.08 s, RF sweep rate = 0.8 MHz/s, microwave power = 2.5 nW, $g_y = 2.005$. These spectra were slightly shifted in the direction of the sweep by the effect of the time constant. The deuterium features were nonexistent in the protonated sample. This spectrum took 85 min of signal averaging.

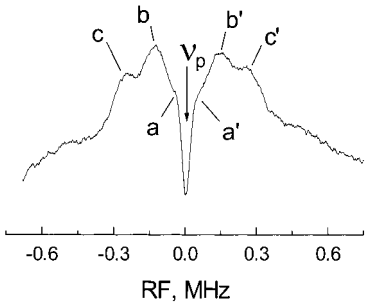

FIGURE 6: This figure provides the Q-band ENDOR signal of protons taken over a 1.5 MHz range centered at the free proton frequency to show features a,a′, b,b′, and c,c′ with weak couplings of 0.09, 0.27, and 0.50 MHz, respectively. Experimental conditions were $T = 2.1$ K, 100 kHz modulation = 0.15 G ptp, system time constant = 0.10 s, RF sweep rate = 0.5 MHz/s, microwave power = 83 nW, $\nu_e = 34.088$ GHz, magnetic field = 12 140 G. This spectrum took 13 min of signal averaging. See Figure S-3 for the derivative presentation of this spectrum.

to protons of the nearby protein and *not* due to weakly coupled protons of the ubisemiquinone.

DISCUSSION

We summarize our experimental and empirical findings: The $Q_H^{\bullet-}$ site presented a characteristic ubisemiquinone anion Q-band EPR spectrum similar to that reported for ubisemiquinone anion in photosynthetic reaction centers and in polar organic solvent (*9*, *10*, *41*, *44*). However, as shown at 90 K (Figure 2) and 2.1 K (Figure 3), nonexchangeable proton features with couplings in the range 9.5−13 MHz were observed, and these couplings are larger than those reported from ubisemiquinone anion elsewhere. A coupling of the order 11 MHz is consistent with 4 G splittings previously observed in X-band EPR spectra (ref *1*, Figure 1a,c) and resolved here in the second-derivative Q-band EPR spectrum. The simulation of the Q-band 90 K second-derivative Q-band EPR spectrum (Figure 1B,B′), using g values determined from Q-band EPR and a proton hyperfine tensor with components in the 9−12 MHz range, required three equivalent protons. Other nonexchangeable proton ENDOR features with couplings in the 2−5 MHz range were resolved at both nitrogen and liquid helium temperatures. From previous work on ubisemiquinone and other semiquinones having long hydrocarbon chains and methyl groups, respectively at the 2 and 3 positions, it is evident that the nonexchangeable proton couplings ≥2 MHz have been either from the ring methyl or from the β-methylene isoprenyl protons (*9*, *10*, *15*, *17*). For such ring protons, there is an anisotropic dipolar contribution of ∼3 MHz as well as an isotropic hyperfine coupling, both primarily due to spin on the adjacent α-carbon. The contribution of the dipolar coupling will be negative when measured at the g_z tensor component perpendicular to the quinone plane. For both features I, I′ and features II, II′, minimal hyperfine couplings were indeed measured at g_z, and the hyperfine anisotropy as a function of g value was of the order 3 MHz; the implication is that features I, I′ and II, II′ are from ubisemiquinone ring methyl or β-methylene isoprenyl protons. Next, there was definitive deuteron evidence of exchangeable deuterons with ∼0.8 MHz coupling (Figure 5). We found possible evidence for a more weakly coupled exchangeable proton with hyperfine coupling of about 1.8 MHz from the starred feature (Figure 4). The evidence from exchangeable proton/deuterons is highly consistent with $Q_H^{\bullet-}$ being hydrogen bonded to its protein surroundings, probably through one or both of its oxygens, O(4) and O(1). As a probe for the protein surroundings, we observed small proton couplings (a,a′; b,b′; c,c′ < 1 MHz) which, based on the detailed results of similar weak couplings of $Q_A^{\bullet-}$ and $Q_B^{\bullet-}$ in photosynthetic reaction centers (ref *10*, Table 1), indicate coupling to protons on nearby, although as yet unidentified, amino acids.

The selective assignment of nonexchangeable features with couplings of 9.5−13 MHz and of 2−5 MHz, explicitly to ring methyl or to β-methylene isoprenyl protons, was not immediately obvious. Therefore, before presenting our rationale for assignment, we first provide an outline of previous relevant findings on ubisemiquinones having ring methyl and β-methylene isoprenyl protons. The couplings of β-methylene isoprenyl protons were reported at 3 °C from single crystals of photosynthetic reaction centers containing $Q_A^{\bullet-}$. These couplings were in the 5−8.5 MHz range (ref *41*, Figure 24). From solutions of reaction centers at −20 °C, the β-methylene isoprenyl protons were reported to have $A_\perp = 5.1$ MHz and $A_\parallel = 8.4$ MHz (*9*). The ring methyl protons were reported from single crystals of photosynthetic reaction centers at 3 °C to have couplings in the 3−6.5 MHz range (ref *41*, Figure 24) and from frozen solutions of reaction centers at 120 K to have $A_\perp = 4.1$ MHz and $A_\parallel = 7.2$ MHz (*9*, *10*). Thus, in both cases the hyperfine couplings of β-methylene isoprenyl and ring methyl protons were approximately equal, and A_{iso} for both types of protons was about 6 MHz. [A slightly larger spin coupling to the β-methylene isoprenyl has been suggested to occur because selective hydrogen bond stabilization of the negative change on O(4) leads, by a simple valence bond description (*45*) or by a more elaborate density functional calculation (*46*), to preferential electron spin density on C(4), C(2), and C(6).] Both the β-methylene isoprenyl protons and the ring methyl protons are located on β-carbons adjacent to an α-carbon of the quinone ring that has π spin density. The predominant isotropic Fermi component, A_{iso}, of hyperfine coupling to a β-proton depends on the unpaired spin density in the π orbital on the α-carbon, and it depends on the square of the cosine of the dihedral angle formed by the $C\alpha-C_\beta-H_\beta$ plane and

the π-C$_\alpha$−C$_\beta$ plane (*47*): $A_{iso} = \rho_C(B_0 + B_2 \cos^2 \theta)$, where ρ_C is the spin density on the adjacent α-carbon, B_0 is close to 0, and B_2 has been taken in the range from 120 (*15*) to 212 MHz (*17*). At liquid nitrogen temperature and above, the methyl groups rotate sufficiently fast to average $\cos^2 \theta$ to 1/2, so that the isotropic coupling for a methyl proton would be $A_{iso} = \rho_C B_2/2$. An isotropic coupling of 6 MHz for the methyl group provides 6−10% of an unpaired spin on the adjacent α-carbon. Even in solution near room temperature the β-methylene isoprenyl is hindered in its motion (*48*). Analysis of β-methylene isoprenyl couplings in ref *15* indicated that the methylene isoprenyl C3−C2−Cβ−Cγ carbon dihedral angle of 90° is favored by ∼6 kcal/mol over the methylene isoprenyl C3−C2−Cβ−Cγ dihedral angle of 0° or 180°, apparently due to the steric clash with the nearby methyl group. With the stabilized C3−C2−Cβ−Cγ dihedral angle of 90°, the β-methylene isoprenyl π-C2−Cβ−Hβ dihedral angles lie at ±60° ($\cos^2 \theta = 1/4$). With the less stabilized C3−C2−Cβ−Cγ dihedral angle of 0° or 180°, the β-methylene isoprenyl π-C2−Cβ−Hβ dihedral angles lie at 30° or 150° ($\cos^2 \theta = 3/4$). [In photosynthetic reaction centers, it was reported (*15*) that the C3−C2−Cβ−Cγ dihedral angles were 82° so that the π-C2−Cβ−Hβ dihedral angles would be approximately 50° and −70°.] If any of the equivalent protons that we observe having couplings of ∼11 MHz were to be β-methylene isoprenyl protons, we would be faced with two possible choices, both of which we disfavor. Either their π-C2−Cβ−Hβ dihedral angles would be ±60°, and an unacceptably high π spin density >20% on the isoprenyl C(2) would be predicted, or the π-C2−Cβ−Hβ dihedral angles would be 30° or 150°, and the energetically less stable conformation of the isoprenyl chain would occur. Furthermore, our Q-band simulations favor three equivalent β-protons in order to predict features of the Q-band second-derivative EPR line shape, and the isoprenyl side chain could only provide two such β-protons.

Isotropic couplings of 10 MHz have been resolved by ENDOR of the phylloquinone (vitamin K) electron acceptor anion radical in photosystem I (*17*). Like ubiquinone, this quinone has a long-chain carbon tail attached at quinone C(2) and a methyl at C(3). Interestingly, hyperfine inflections in the X-band EPR spectrum of phylloquinone (ref *18*, Figure 2) and of $Q_H^{\bullet-}$ (ref *1*, Figure 1a,c) bear resemblance. Because *three* equivalent protons having couplings consistent with our ENDOR results in the 9−13 MHz range account for the detailed hyperfine features in our second-derivative Q-band EPR spectrum at 90 K, we assign the protons I, I′ with this coupling in the 9−13 MHz range to the ubisemiquinone methyl protons. A value of $A_{iso} = 11$ MHz for methyl protons would imply that the π spin density on C(3) adjacent to the methyl group is 11−18% (depending on choice of the parameter B_2), about double that found for ubisemiquinone methyls in the photosynthetic reaction center. The couplings of nonexchangeable protons in the 2−5 MHz regime are thus assigned to the β-methylene isoprenyl protons; so the spin density on C(2) would be somewhat smaller than found for β-methylene isoprenyl protons in the photosynthetic reaction centers.

CONCLUSION

The Q-band EPR spectrum of $Q_H^{\bullet-}$ was determined to be from a ubisemiquinone anion with *g* values similar to those of ubisemiquinone in the photosynthetic reaction centers. However, the details of hyperfine coupling to nonexchangeable protons were decidedly different from those of photosynthetic reaction centers. The most notable difference was the nonexchangeable proton hyperfine coupling of 9.5−13 MHz (features I, I′), which is larger than any proton coupling observed in ubisemiquinone of the photosynthetic reaction centers. Because the fit to hyperfine features in the Q-band second-derivative EPR spectrum required three such equivalent protons with this large coupling, we assigned these protons to the ubiquinone methyl group. Such an assignment implies a larger spin density on the α-carbon C(3) adjacent to the ring methyl than is found in the ubisemiquinones of the photosynthetic reaction center. Nonexchangeable protons with coupling of 2−5 MHz (features II, II′) were thus assigned to the β-methylene isoprenyl protons, and such an assignment implies a smaller spin density on the α-carbon C(2) adjacent to the isoprenyl chain than is found in the ubisemiquinones of the photosynthetic reaction center. The alteration in spin density suggests a preferential stabilization of negative charge on O(1) in contrast to the slightly greater stabilization of negative charge on O(4) in photosynthetic reaction centers (*46*, *49*). Deuteron ENDOR gave definitive evidence for exchangeable protons/deuterons consistent with hydrogen bonding to the quinone oxygen(s), hydrogen bonding that could be accomplishing this stabilization of O(1). Evidence of weak proton couplings to the surroundings indicated protons of the nearby protein matrix. So that in the future we can delineate critical neighboring amino acids whose mutation could alter $Q_H^{\bullet-}$ function, stability, and electronic spin density, the background is now available for future comparison of π electronic spin distribution, exchangeable deuterons/protons, and weak couplings to protons of the nearby protein surroundings.

SUPPORTING INFORMATION AVAILABLE

The following figures are included: Supplementary Figures S-1 and S-2 present a more detailed, close-up of the change of hyperfine coupling to feature I′ (assigned to quinone methyl) as a function of *g* value; S-1 is from a protonated sample, and S-2 is from a deuterated sample. Figure S-3 shows by a derivative presentation the elucidation of the weak couplings initially shown in Figure 6 of the text (4 pages). This material is available free of charge via the Internet at http://pubs.acs.org.

REFERENCES

1. Ingledew, W. J., Ohnishi, T., and Salerno, J. C. (1995) *Eur. J. Biochem. 227*, 903−908.
2. Mitchell, P. (1975) *FEBS Lett. 59*, 137−139.
3. Mitchell, P. (1976) *J. Theor. Biol. 62*, 327−367.
4. Beroza, P., Fredkin, D. R., Okamura, M. Y., and Feher, G. (1995) *Biophys. J. 68*, 2233−2250.
5. Deisenhofer, J., Epp, O., Miki, K., Huber, R., and Michel, H. (1985) *Nature 318*, 618−624.
6. Allen, J. P., Feher, G., Yeates, T. O., Komiya, H., and Rees, D. C. (1987) *Proc. Natl. Acad. Sci. U.S.A. 84*, 6162−6166.
7. Feher, G., Allen, J. P., Okamura, M. Y., and Rees, D. C. (1989) *Nature 339*, 111−116.
8. Stowell, M. H. B., McPhillips, T. M., Rees, D. C., Soltis, S. M., Abresch, E., and Feher, G. (1997) *Science 276*, 812−816.
9. Feher, G., Isaacson, R. A., Okamura, M. Y., and Lubitz, W. (1985) in *Antennas and Reaction Centers of Photosynthetic*

Bacteria—Structure, Interactions and Dynamics (Michel-Beyerle, M. E., Ed.) pp 174−189, Springer-Verlag, Berlin.
10. Lubitz, W., Abresch, E. C., Debus, R. J., Isaacson, R. A., Okamura, M. Y., and Feher, G. (1985) *Biochim. Biophys. Acta 808*, 464−469.
11. Isaacson, R. A., Abresch, E., Feher, G., Lubitz, W., Williams, J. C., and Allen, J. P. (1995) *Biophys. J. (Abstr.) 68*, A246.
12. Bosch, M. K., Gast, P., Hoff, A. J., Spoyalov, A. P., and Tsvetkov, Y. D. (1995) *Chem. Phys. Lett. 239*, 306−312.
13. MacMillan, F., Lendzian, F., Renger, G., and Lubitz, W. (1995) *Biochemistry 34*, 8144−8156.
14. Rigby, S. E. J., Heathcote, P., Evans, M. C. W., and Nugent, J. H. A. (1995) *Biochemistry 34*, 12075−12081.
15. Zheng, M., and Dismukes, B. C. (1996) *Biochemistry 35*, 8955−8963.
16. Deligiannakis, Y., Hanley, J., and Rutherford, A. W. (1999) *J. Am. Chem. Soc. 121*, 7653−7664.
17. Rigby, S. E. J., Evans, M. C. W., and Heathcote, P. (1996) *Biochemistry 35*, 6651−6656.
18. MacMillan, F., Hanley, J., van der Weerd, L., Knüpling, M., Un, S., and Rutherford, A. W. (1997) *Biochemistry 36*, 9297−9303.
19. Hanley, J., Deligiannakis, Y., MacMillan, F., Bottin, H., and Rutherford, A. W. (1997) *Biochemistry 36*, 11543−11549.
20. Ingledew, W. J., Salerno, J. C., and Ohnishi, T. (1976) *Arch. Biochem. Biophys. 177*, 176−184.
21. Kotlyar, A. B., Sled, V. D., Burbaev, D. Sh., Moroz, J. A., and Vinogradov, A. D. (1990) *FEBS Lett. 347*, 22−26.
22. De Vries, S., Albracht, S. P. J., Berden, J. A., and Slater, E. C. (1982) *J. Biol. Chem. 256*, 11996−11998.
23. De Vries, S., Albracht, S. P. J., Berden, J. A., and Slater, E. C. (1982) *Biochim. Biophys. Acta 681*, 41−53.
24. Jünemann, S., Heathcote, P., and Rich, P. R. (1998) *J. Biol. Chem. 273*, 21603−21607.
25. Xia, D., Yu, C. A., Kim, H., Xia, J.-Z., Kachurin, A. M., Zhang, L., Yu, L., and Deisenhofer, J. (1997) *Science 277*, 60−66.
26. Zhang, Z., Huang, L., Shulmeister, V. M., Chi, Y.-I., Kim, K. K., Hung, L.-W., Crofts, A. R., Berry, E. A., and Kim, S.-H. (1998) *Nature 392*, 677−684.
27. Puustinen, A., Finel, M., Haltia, T., Gennis, R. B., and Wikström, M. (1991) *Biochemistry 30*, 3936−3942.
28. Puustinen, A., and Wikström, M. (1991) *Proc. Natl. Acad. Sci. U.S.A. 38*, 6122−6126.
29. Puustinen, A., Morgan, J. E., Verkhovsky, M., Thomas, J. W., Gennis, R. B., and Wikström, M. (1992) *Biochemistry 31*, 10363−10369.
30. Sato-Watanabe, M., Mogi, T., Ogura, T., Kitagawa, T., Miyoshi, H., Iwamura, H., and Anraku, Y. (1994) *J. Biol. Chem. 269*, 28908−28912.
31. Sato-Watanabe, M., Itoh, S., Mogi, T., Matsuura, K., Miyoshi, H., and Anraku, Y. (1995) *FEBS Lett. 374*, 265−269.
32. Puustinen, A., Verkhovsky, M. I., Morgan, J. E., Belevich, N. P., and Wikström, M. (1996) *Proc. Natl. Acad. Sci. U.S.A. 93*, 1545−1548.
33. Schultz, B. E., and Chan, S. I. (1998) *Proc. Natl. Acad. Sci. U.S.A. 95*, 11643−11648.
34. Schultz, B. E., Edmondson, D. E., and Chan, S. I. (1998) *Biochemistry 37*, 4160−4168.
35. Rumbley, J. N., Nickels, E. F., and Gennis, R. B. (1997) *Biochim. Biophys. Acta 1340*, 131−142.
36. Osborne, J. P., Cosper, N. J., Stalhändske, C. M. V., Scott, R. A., Alben, J. O., and Gennis, R. B. (1999) *Biochemistry 38*, 4526−4532.
37. Sienkiewicz, A., Smith, B. G., Veselov, A., and Scholes, C. P. (1996) *Rev. Sci. Instrum. 67*, 2134−2138.
38. Scholes, C. P., Falkowski, K. M., Chen, S., and Bank, J. (1986) *J. Am. Chem. Soc. 108*, 1660−1671.
39. Feher, G., Okamura, M. Y., and McElroy, J. D. (1972) *Biochim. Biophys. Acta 244*, 222−226.
40. Burghaus, O., Plato, M., Rohrer, M., Möbius, K., MacMillan, F., and Lubitz, W. (1993) *J. Phys. Chem. 97*, 7639−7647.
41. Feher, G. (1998) *Photosynth. Res. 55*, 1−40.
42. Okamura, M. Y., Isaacson, R. A., and Feher, G. (1975) *Proc. Natl. Acad. Sci. U.S.A. 72*, 3491−3495.
43. Kevan, L., and Kispert, L. D. (1976) *Electron Spin Double Resonance Spectroscopy*, pp 218−222, Wiley-Interscience, New York.
44. O'Malley, P. J., and Babcock, G. T. (1986) *J. Am. Chem. Soc. 108*, 3995−4001.
45. Van den Brink, J. S., Spoylaov, A. P., Gast, P., van Liemt, W. B. S., Raap, J., Lugtenburg, J., and Hoff, A. J. (1994) *FEBS Lett. 353*, 273−276.
46. O'Malley, P. J. (1998) *J. Phys. Chem. A 102*, 248−253.
47. Atherton, N. M. (1973) *Electron Spin Resonance*, pp 103−108, Wiley & Sons, Inc., New York.
48. Das, R., Connor, H. D., Leniart, D. S., and Freed, J. H. (1970) *J. Am. Chem. Soc. 92*, 2258−2268.
49. Van Liemt, W. B. S., Boender, G. J., Gast, P., Hoff, A. J., Lugtenburg, J., and de Groot, H. J. M. (1995) *Biochemistry 34*, 10229−10236.

BI9926835